Supporting Information

Rational synthesis of hollow cubic CuS@Spiky Au core-Shell nanoparticles for enhanced photothermal and SERS Effects

Qian Lv, Meng-Yue Gao, Zi-He Cheng, Qiao Chen, Ai-Guo Shen* and Ji-Ming Hu

Key Laboratory of Analytical Chemistry for Biology and Medicine (Ministry of Education), College of Chemistry and Molecular Sciences, Wuhan University, Wuhan 430072, PR China

TABLE OF CONTENTS

EXPERIMENTAL SECTION

Materials: All chemicals obtained from commercial suppliers were used without further purification. Ultrapure water (Millipore Milli-Q grade) with an electrical resistivity of 18.2 MΩ was used throughout the work. All glass was cleaned with aqua regia. Poly(vinylpyrrolidone) (PVP, MW~10000), PVP-K30 hydrogen tetrachloroaurate (Ⅲ) trihydrate ($HAuCl_4.3H_2O$)，cresyl violet acetate (CVa) were purchased from Aladdin industrial corporation. Ascorbic acid (AA), sodium hydroxide (NaOH), hydroquinone, cupric acetate monohydrate ($Cu(Ac)_2.H_2O$), Sodium sulfide nonahydrate ($Na_2S.9H_2O$) were purchased from Sinopharm Chemical Reagent CO., Ltd.

Characterization: Scanning electron microscope (SEM) images were obtained with a filed-emission scanning electron microscopy (FE-SEM, SIGMA). Transmission electron microscopy (TEM) and High resolution TEM (HRTEM) images were collected on a JEM-2100 (JEOL) microscope. Element mapping and energy dispersive spectroscopy (EDS) were performed on FEI Tecnai G2 F20 STwin microscope working at 200 kV equipped with X-ray energy dispersive spectroscopy detector (XEDS). A JEM-ARM200F STEM fitted with a double aberration-corrector for both probe-forming and imaging lenses is used to perform HAADF imaging, which was operated at 200 kV. Raman spectra was collected from Jobin Yvon Raman micro spectrometer (HR800), equipped with a 632.8 nm excitation laser and a 20 and 50 Lx objective lens. X-ray power diffraction (XRD) patterns were characterized with a Shimadzu XRD-6000 X-ray diffractometer equipped with Cu Kα1 radiation (λ = 0.15406 nm). When SERS images of the label-free NPs were generated, the scan over cells was carried out on a computer-controlled XY stage in 6 μm steps. The power density of 633 nm laser was 1.2×10^4 W/cm^2 in SERS mapping. SERS images were generated using the integrated signal-to-baseline intensity from 490 to 1650 cm^{-1}. Dynamic light scattering (DLS) data was measured by a Nano-ZSP90 (Malvern Instruments). UV-Vis-NIR spectrums of samples were recorded using Shimadzu UV-2550 spectrophotometer.

Synthesis of hollow cubic CuS nanoparticles (HCCuS NPs): 100 mL mixed solution of 0.5% poly(vinylpyrrolidone) (PVP, MW~10000) and 0.5 mM $Cu(Ac)_2$ was gently stirred for 15 min at room temperature. Then 900 μL of NaOH (1 M) solution was added into the above solution. After stirring for 2 min, AA (0.1 M, 1.5 mL) was added to the above mixture dropwise and stirred for another 5 min. The mixtures were left undisturbed for 30 min under room temperature. Then, the temperature was improved to 90°C. Under stirring, Na_2S (0.05 M, 2 mL) was added and the reaction was continued for 2 h. After

reaction, the product was purified by centrifugation (7500 rpm, 15 min) and washed with deionized water three times.

Synthesis of hollow spherical CuS nanoparticles (HSCuS NPs): Briefly, $Cu(Ac)_2$ solution (100 μL, 0.1 M) was added to deionized water (50 mL) containing poly(vinylpyrrolidone) (PVP-K30, 0.3 g) under magnetic stirring at room temperature. Then, NaOH solution (25 mL, pH ~9.0) was added, followed by addition of hydrazine anhydrous solution (10 μL) to form a suspension of Cu_2O spheres. After 5 min, Na_2S aqueous solution (500 μL, 0.1 M) was added to the suspension. Then the solution was heated for 4 h at 60°C. HSCuS NPs were centrifuged at 6500 rpm for 30 min and washed twice with distilled water.

Synthesis of hollow cubic CuS@Au with different morphologies of Au shell: The 10 mL of the above CuS solution was diluted to 20 mL aqueous solution. 2 mL AA (0.1 M) was injected to the CuS solution under strong magnetic stirring. After stirring for 15 min, 4 mM of $HAuCl_4$ solution (6 mL) was added by dropwise to the mixed solution. After 30 min at room temperature, the HCCuS@Spiky Au NPs were formed and collected by centrifugation (3000 rpm, 5 min) and washed with deionized water three times. HCCuS@Dotted Au NPs and HCCuS@Islandeded Au NPs were obtained by using 4 mL and 8 mL of $HAuCl_4$ aqueous solution, respectively.

Synthesis of hollow spherical CuS@Au with different morphologies of Au shell: The 10 mL of the above CuS solution was diluted to 20 mL aqueous solution. 2 mL AA (0.1 M) was injected to the CuS solution under strong magnetic stirring. After stirring for 15 min, 4 mM of $HAuCl_4$ solution (4 mL) was added by dropwise to the mixed solution. After 30 min at room temperature, the HSCuS@Spiky Au NPs were formed and collected by centrifugation (3000 rpm, 5 min) and washed with deionized water three times. HSCuS@Dotted Au NPs and HSCuS@Islandeded Au NPs were obtained by using 2 mL and 6 mL of $HAuCl_4$ aqueous solution, respectively.

The evolution of the HCCuS@Au with different morphologies of Au shell from dots to branches to islands: When the molar ratio of $HAuCl_4$ to AA was equal to 1:10, HCCuS@Au nanostructures (HCCuS@Dotted Au NPs) with a Dotted Au nanoparticle surface were prepared (Fig. 1(A1)). HCCuS@Au nanostructures (HCCuS@Spiky Au NPs) with a Spiky Au shell surface (Fig. 1(A2)) were synthesized by tuning the molar ratio of $HAuCl_4$ to AA from 1:10 to 1:6.67. With the increased molar ratio of $HAuCl_4$ to AA reaching 1:5, islands of Au shell coated HCCuS NPs appeared, as shown in Fig. 1(A3).

The discussion of the SPR band position of HCCuS@Au NPs in UV-vis spectra (HCCuS@Dotted Au NPs, HCCuS@Spiky Au NPs, HCCuS@Islanded Au NPs): The increased molar ratio of $HAuCl_4$ to AA in the synthesis resulted in a branch tip structure of gold shells coating the CuS core, of which the LSPR peak was red-shifted from that of HCCuS@Dotted Au NPs because of the branch "tip spots". Blue-shifting was observed for HCCuS@Islanded Au NPs prepared when the molar ratio of $HAuCl_4$ to AA was equal to 1:5 due to the disappearance of strong "tip spots" as compared to HCCuS@Spiky Au NPs.

These SPR bands are strongly governed by particle shape, size, composition and the surrounding medium.[1,2] Detailed discussion of the UV-vis spectra of the above-mentioned NPs are as follows:

Upon the gold growth, SPR bands of all kinds of HCCuS@Au NPs were blue-shifted compared to that of pure HCCuS nanocrystals (about 950 nm), which were attributed to plasmonic coupling between Au nanocrystals and CuS core.[3] To our knowledge, the SPR band of Au NPs was red-shifted as their size and tip sharpness increased.[4, 5] Besides, the SPR bands of Au NPs with dotted, spiky and islanded shape were around 517, 750 and 600 nm, respectively.[6,7] Thus, the blue-shifted extent of the HCCuS@Au NPs was HCCuS@Dotted Au NPs> HCCuS@Islanded Au NPs> HCCuS@Spiky Au NPs. Thus, HCCuS@Dotted Au NPs, HCCuS@Islanded Au NPs, and HCCuS@Spiky Au had SPR band around 700, 750 and 800 nm, respectively. As the HCCuS@Islanded Au NPs were changed from HCCuS@Spiky Au NPs, the grew gold crystals filled up the gap between the branched gold tips, and the considered thick gold shell (island gold) achieved finally. And the SPR band of the island gold shell (near 600 nm) became impossible to ignore compared to the SPR of pure CuS core.[7,8] In general, the SPR bands have closely relation with the morphology of the NPs.

The calculation of the analytical enhancement factor (AEF): The analytical enhancement factor (AEF) can be defined as equation:

$$AEF = \frac{I_{SERS}/C_{SERS}}{I_{RS}/C_{RS}}$$

Where, I_{SERS} and I_{RS} are the intensity of the enhanced SERS sample and from the blank dye molecular (CVa), while C_{SERS} and C_{RS} are the analyte concentration in the SERS experiment and the analyte concentration in the normal Raman experiment.

According to this established definition, the AEF of the HCCuS@Spiky Au NPs was established by considering the 591 cm^{-1} Raman band, because it is the strongest peak of all bands in the spectra. When using the $C_{SERS}=10^{-6}$ M and $C_{RS}=10^{-2}$ M and the intensities obtained from Figure 2E, we can obtain a value of AEF=1.2×10^{6}.

Measurement of photothermal effect: A NIR laser (808 nm, BWT Beijing Ltd.) was used during the photothermal effect measurements and the following *in vitro* PTT experiments. The hollowed cubic CuS@Au aqueous solution was placed in a quartz cuvette at a series of concentrations and was exposed to the NIR laser (808 nm, 0.45 W/cm^2) for 5 min. Simultaneously, a thermocouple probe connected to a digital thermometer (with an accuracy of 0.1˚C) was inserted into the solution to measure the real-time temperature, and the change of temperature was recorded every 30 s.

To evaluate the photothermal conversion efficiency, the temperature change of the aqueous dispersion (50 ppm) was recorded as a function of time under continuous irradiation of the 808 nm laser with a power density of 0.45 W/cm^2 until the solution reached a steady-state temperature. The photothermal conversion efficiency, i.e. η, was calculated using eq 1 described by Roper: where h is the heat transfer coefficient, S is the surface area of the container, T_{max} is the equilibrium temperature, T_{surr} is the ambient temperature, Q_{dis} expresses the heat dissipation from the light absorbed by the quartz sample cell, I is incident laser power (0.45 W/cm^2), and A_{808} is the absorbance of the HCCuS@Dotted Au, HCCuS@Spiky Au and HCCuS@Islanded Au nanocrystals at 808 nm. The value of hS is derived according to eq 2:

$$\eta = \frac{hs(T_{max} - T_{surr}) - Q_{dis}}{\mathrm{I}(1 - 10^{-A_{808}})} \quad (1)$$

$$\tau_S = \frac{m_D C_D}{hs} \quad (2)$$

where τ_s is the sample system time constant, m_D and C_D are the mass (0.25 g) and heat capacity (4.2 J/g) of deionized water used as the solvent, respectively. The Q_{dis} (25.7 mW) was measured independently using a quartz cuvette cell containing pure water without the nanoparticles.

***In Vitro* Cytotoxicity Assays of the HCCuS@Spiky Au NPs:** A standard MTT assay was conducted using Human cervix carcinoma cell line (HeLa) to evaluate the *in vitro* cytotoxicity of the NPs. Typically, HeLa cells (1.5×10^{4}/well) were seeded into 96-well plates, and then the cells were incubated in the culture

medium for 12 h at 37˚C under 5% CO_2 atmosphere. The culture medium was then removed, and the cells were incubated with fresh medium containing 100 μL of the NPs at varied concentrations (0, 6.25, 12.5, 25, 50, 100, and 200 ppm) at 37˚C under 5% CO_2 for an additional 24 h and 48 h. Subsequently, the cells were washed twice with PBS and cultured in DMEM supplemented by 10% FBS. Then, 100 μL MTT was added and allowed to react with the cells for 4 h before the addition of 100 μL DMSO to dissolve formazan crystals. Bio-Rad model-680 microplate reader was applied to measure the absorbance at a wavelength of 570 nm (corrected for background absorbance at 490 nm)

In Vitro **Photothermal Therapy of Cancer Cells:** HeLa cells were incubated with seven different concentration NPs for 48 h, then the cells were washed with PBS, followed by 5 min irradiation (808 nm, 0.45 W/cm^2). After another 12 h incubation, the cell viability was evaluated using the MTT assay. A mixed solution containing 2 μM of calcein AM and 4 μM of PI was then added to the wells. After being stained for 30 min, cells were washed with PBS and examined using a fluorescence microscope to observe their live/dead status.

In Vitro **SERS imaging and measure:** For the SERS studies, HeLa cells were grown on glass coverslips for a 70% final confluence at 37˚C for 12 h. Subsequently, the cells were incubated with NPs diluted to the specified concentration in supplemented DMEM for 12 h. After the cells were washed three times with PBS, cells were subsequently irradiated for 5 min using 808 nm laser (0.45 W/cm^2). SERS spectra were acquired using a Jobin Yvon Raman micro spectrometer (HR800), which utilized a 632.8 nm excitation laser (He-Ne laser) and a microscope with a 20× and 50× objective lens. Raman spectra were collected once with 1 s integration time, 1 accumulation over a spectral range from 490 to 1650 cm^{-1}. The step size of SERS intracellular imaging for the large-scale cells and single cell are 8 μm and 2 μm, respectively.

SUPPORTING SCHEME

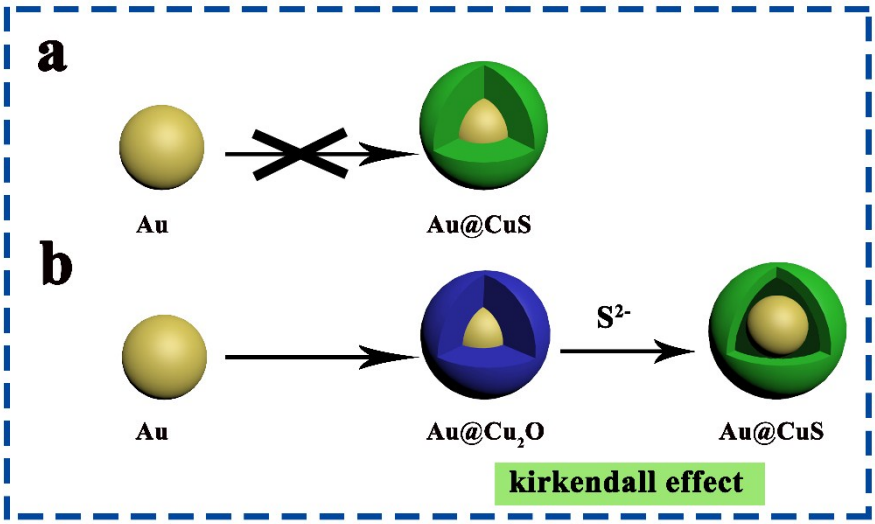

Scheme S1. Synthesis route of Au@CuS core-shell NPs.

Considering the perfect integration of enhanced SERS and photothermal (PT) effect into a unit to a maximum extent, we ultimately determined the optimal synthesis routes and gained the desired nanostructure (hollow cubic CuS@Spiky Au core-shell NPs) for SERS imaging-guided PTT from **Scheme S1 and S2**.

As shown in **Scheme S1a,** one-pot synthesis through heteroepitaxial growth cannot produce monodisperse Au@CuS core-shell NPs because of the large lattice mismatch of Au and CuS.[9] Because Au@Cu_2O core-shell NPs have been produced with a lattice mismatch of 4.5% through epitaxial growth strategies.[10] Herein, the Au@$Cu_{2-x}S$ core-shell NPs were fabricated by means of indirect synthesis. The specific synthetic route was as follows: Cu_2O shell, as the sacrifice template can be first epitaxial growth on the Au core shell, and then the Au@CuS core-shell NPs were gained with the kirkendall effect by the anion exchange between S^{2-} and O^{2-} (**Scheme S1b**). Furthermore, the thickness of CuS shell can be rationally tailored by controlling the amount of the Cu precursor. The photothermal (PT) conversion efficiency of the Au@CuS core-shell NPs is 43.25%, which are much higher than of the reported CuS NPs.[11] However, the configuration of Au core@CuS shell seriously constrained the SERS function due to the exist of the near filed theory. To gain the optimum dual functional effect of PT and SERS, new nanomaterials need to be explored. In the following section, we designed the novel nanostructures for satisfying the dual functional effect.

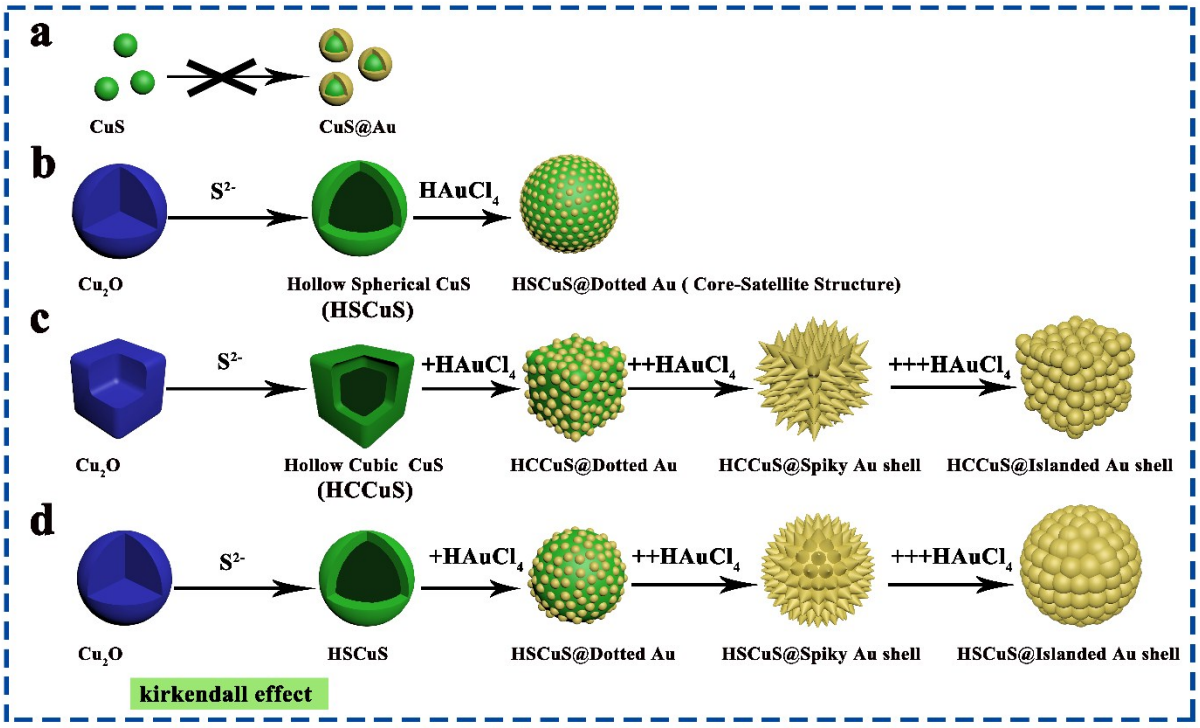

Scheme S2. Synthesis route of CuS@Au core-shell NPs with different Au morphologies.

The CuS@Au core-shell NPs with a spread-out shell cannot also be gained by one-step epitaxial growth method (**Scheme S2a)**, since there is a large interfacial energy between CuS and Au.[8] In **Scheme S2b**, CuS NPs were synthesized by one-step ion exchange with kirkendall effect. The CuS NPs formed by the approach, provided the favorable CuS-Au interface because the PVP coated interface can lower the interfacial energy between CuS and Au and facilitate the nucleation and growth for Au NPs.[12] Thus, the CuS@Au core-satellite NPs had been successfully prepared by the first time (**Scheme S2b)**.[13] The PT conversion efficiency is calculated to 35% under 808 nm laser. The enhanced PT effect of the core-satellite NPs was limited due to not the maximum extent of the LSPR coupling between CuS and Au. Herein, we fabricated a set of CuS@Au NPs by controlling the molar ratio of $HAuCl_4$ to AA. Seen in **Scheme S2c, d**, due to the flexible and independent morphology control of CuS core, the core could be evolved from nanosphere to nanocube with high uniformity, which was used for the Au coated growth. It was note that the CuS@Spiky Au core-shell NPs among these NPs achieved the maximum plasmonic coupling, further enhancing the PT conversion efficiency (~ 62.5%) and the SERS effect. The detailed SERS effect was presented in the main body.

SUPPORTING FIGURE

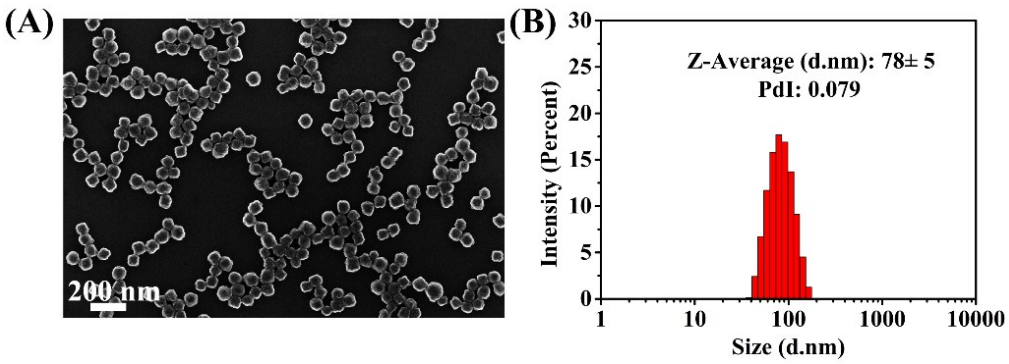

Figure S1. SEM image (A) and size distribution map (B) of HCCuS NPs.

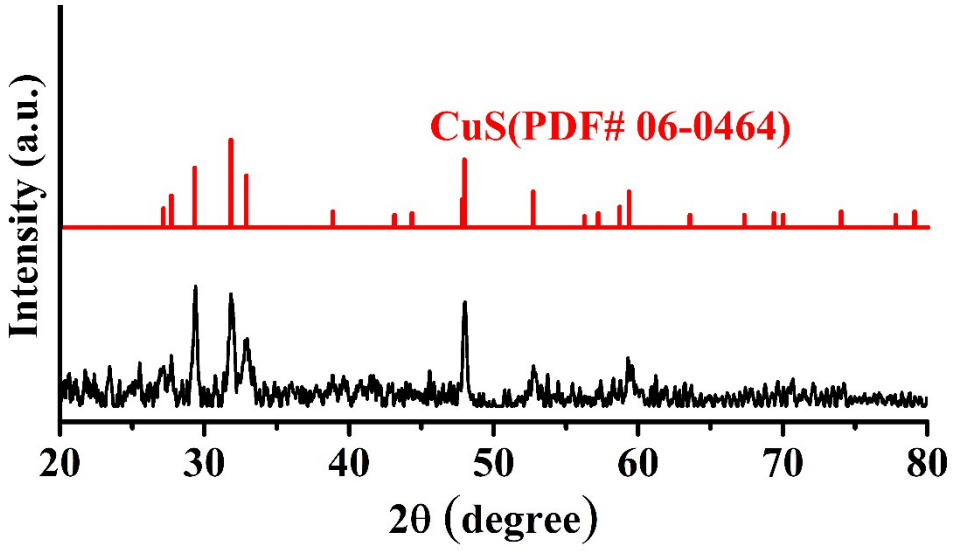

Figure S2. XRD patterns of covellite CuS NPs.

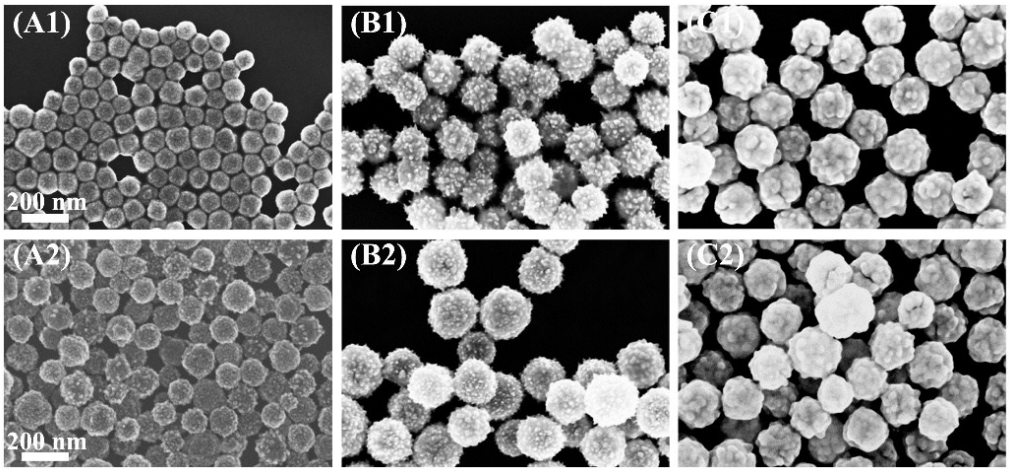

Figure S3. SEM images of (A1-C1) HCCuS@Au and (A2-C2) HSCuS@Au with different morphologies of Au shell NPs synthesized by controlling the molar ratio of $HAuCl_4$ to AA.

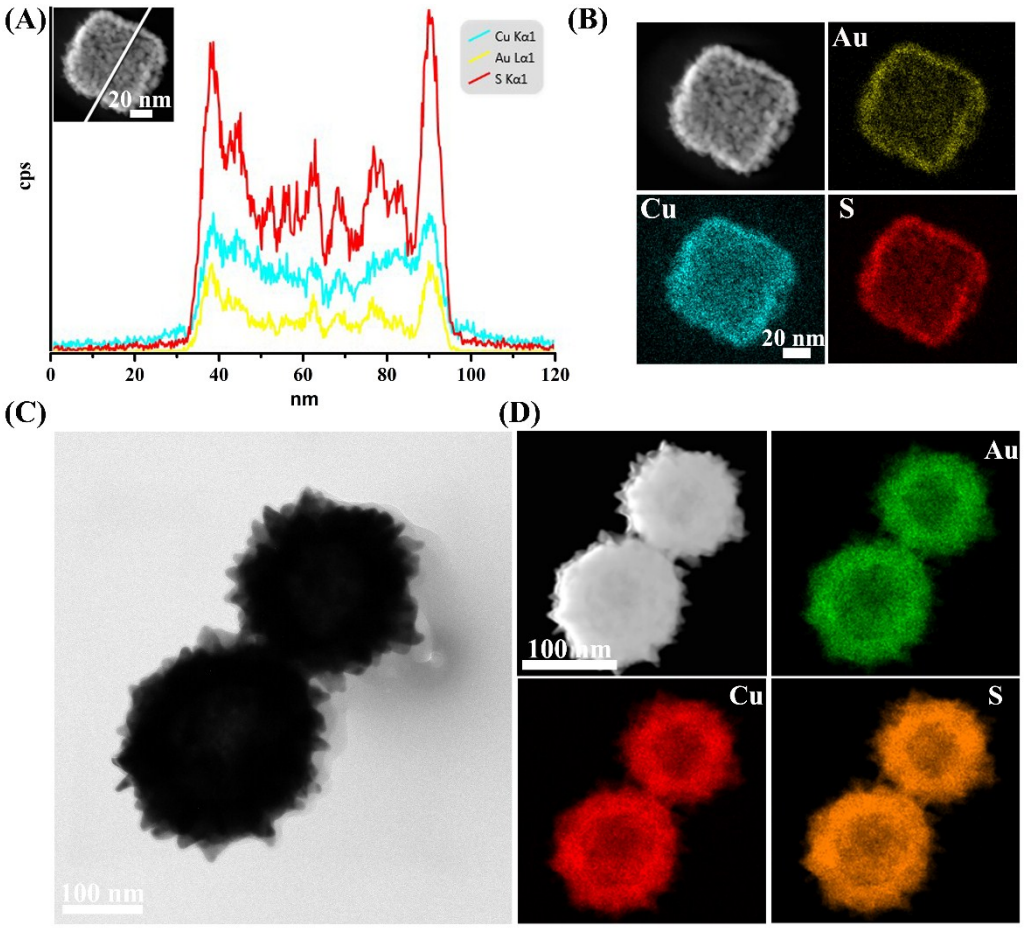

Figure S4. (A) line scanning image and (B) elemental mapping of HCCuS@Dotted Au NPs. (C) TEM image of HCCuS@Spiky Au NPs. (D) STEM image and STEM-EDS elemental mapping images of the HCCuS@Spiky Au NPs in (C).

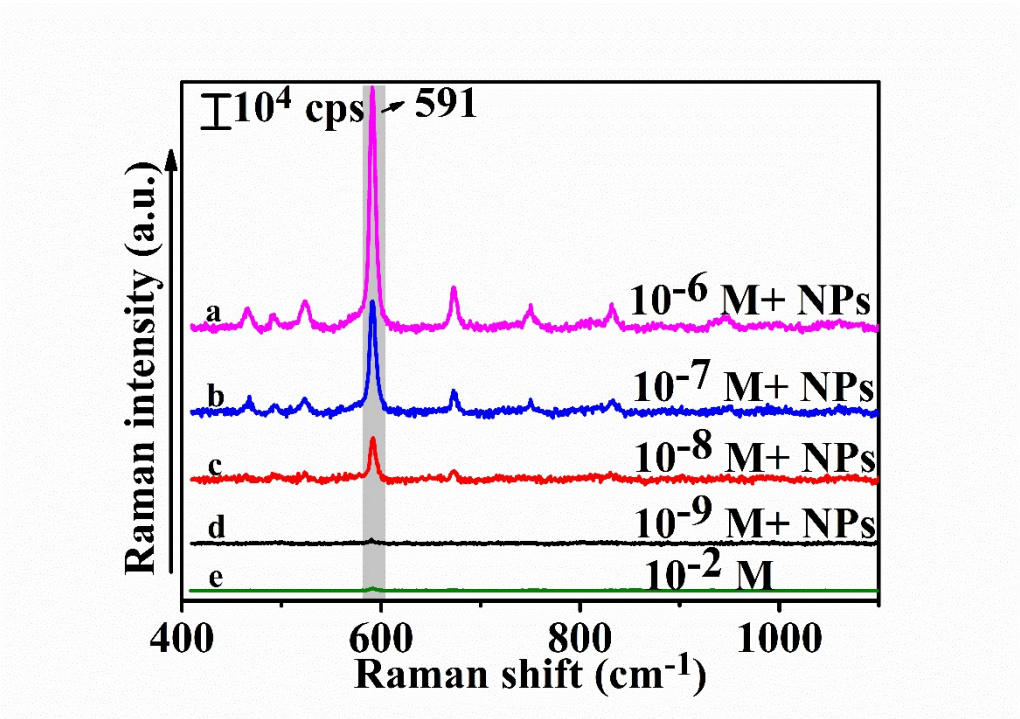

Figure S5. Normal Raman spectra of CVa only and SERS spectra of different concentrations of CVa mixed with the HCCuS@Spiky Au NPs.

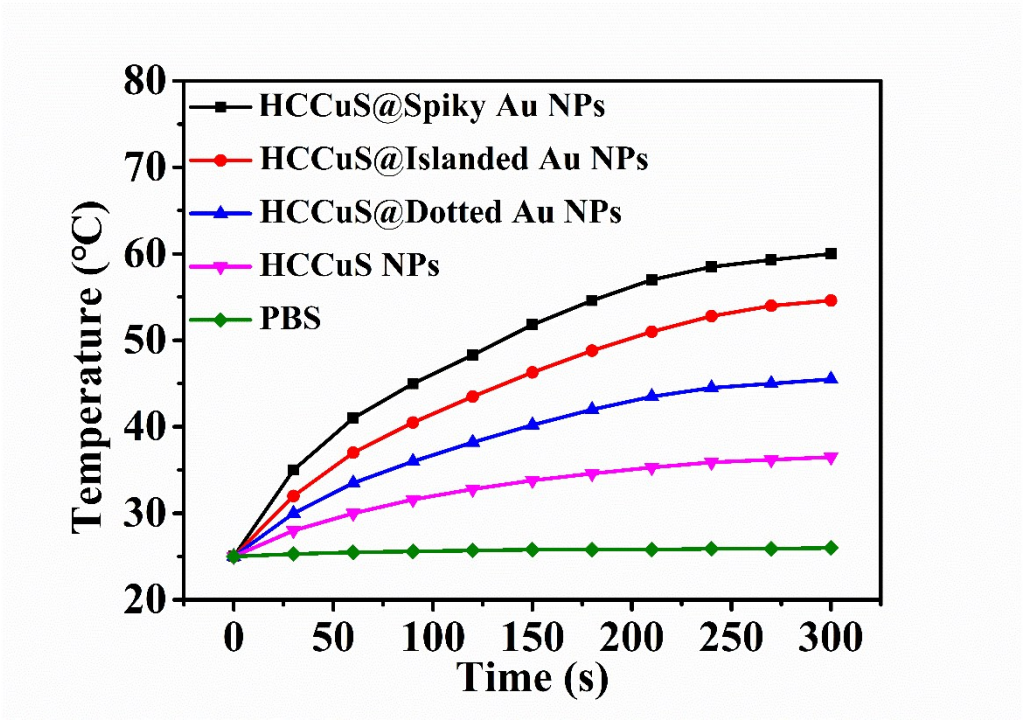

Figure S6. Temperature variation of HCCuS@Dotted Au NPs, HCCuS@Spiky Au NPs, HCCuS@Islanded Au NPs, HCCuS NPs, and PBS as a function of laser (808 nm) irradiation time at 0.45 W/cm^2.

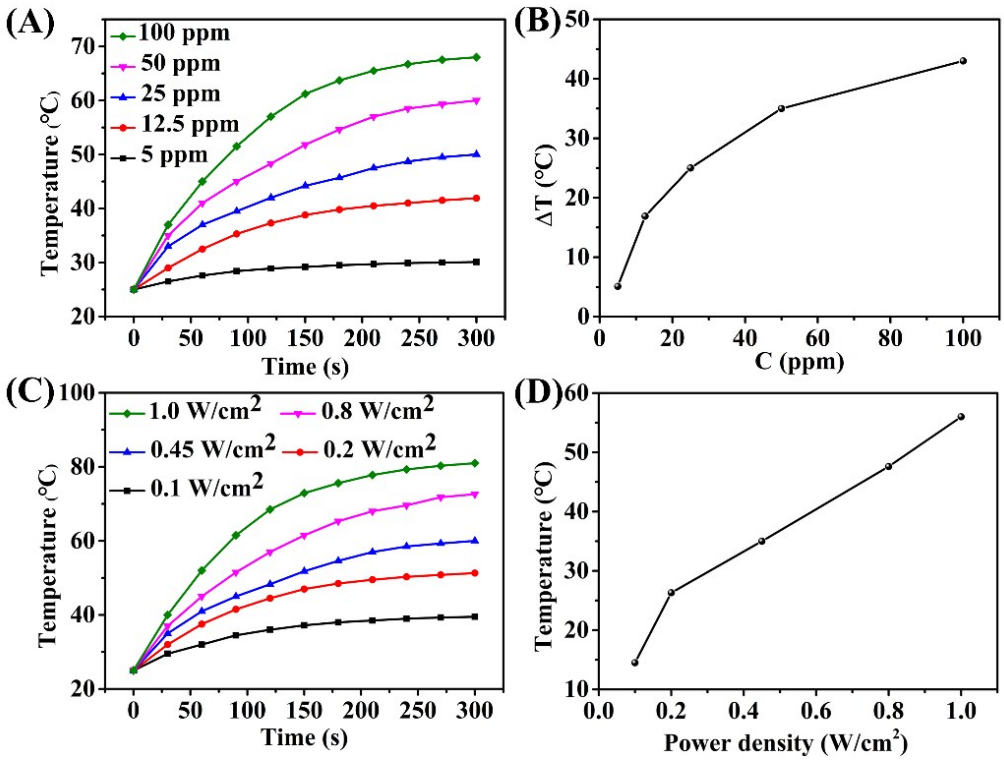

Figure S7. (A) Temperature elevation profiles of HCCuS@Spiky Au NPs dispersed in water with different concentrations after 808 nm laser irradiation (0.45 W/cm^2) for 5 min. (B) Plot of the temperature increase (ΔT) over a period of 5 min versus concentration. (C) Temperature increase curves of HCCuS@Spiky Au NPs in aqueous solution (50 ppm) exposed to 808 nm lasers of different power densities. (D) Plot of temperature change (ΔT) over a period of 5 min versus power density of laser.

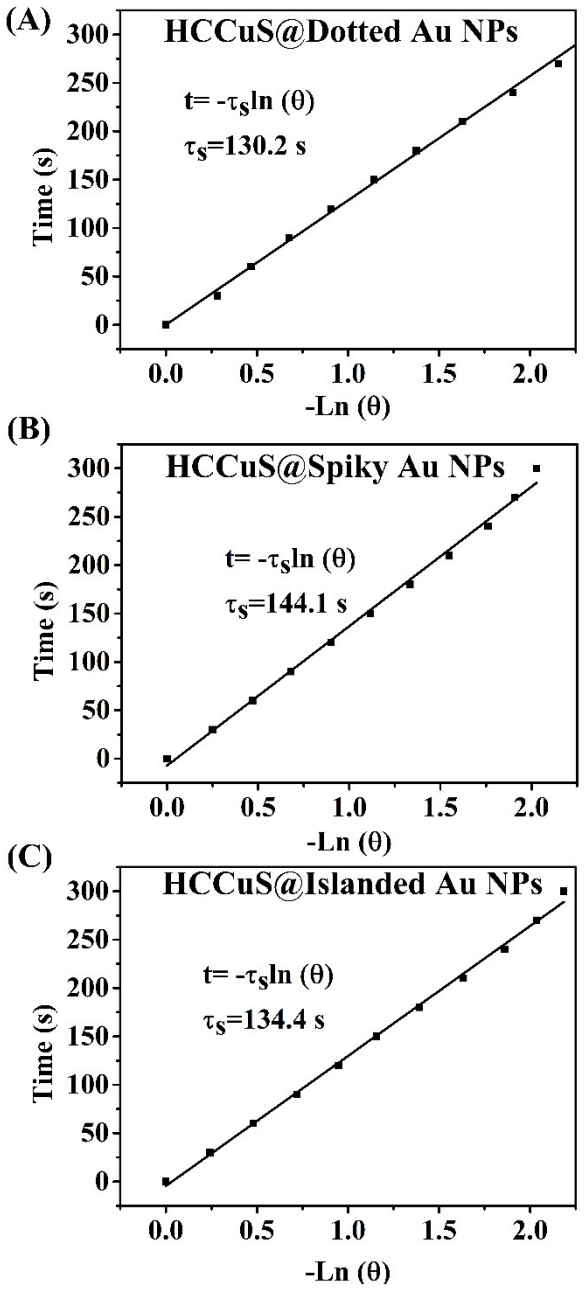

Figure S8. Graph of the cooling period of (A) HCCuS@Dotted Au NPs, (B) HCCuS@Spiky Au NPs, (C) HCCuS@Islanded Au NPs solution after laser irradiation, respectively. The time constant for heat transfer of this system can be obtained by applying linear time data *versus* ln θ from this cooling stage. (Figure 2C). The photothermal conversion efficiencies of HCCuS@Dotted Au NPs, HCCuS@Spiky Au NPs, HCCuS@Islanded Au NPs were calculated to be 35.58%, 52.78%, 62.5%, respectively.

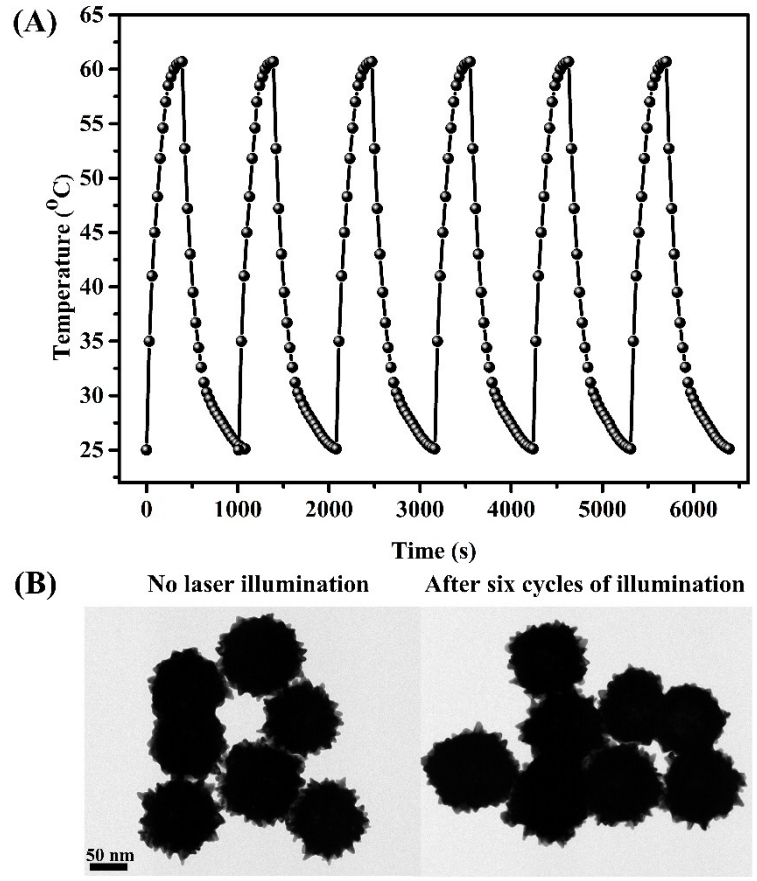

Figure S9. Photothermal stability study of the HCCuS@Spiky Au NPs. (A) Photothermal conversion curves for six cycles. (B) TEM images of the NPs without laser illumination and after six cycles of illumination.

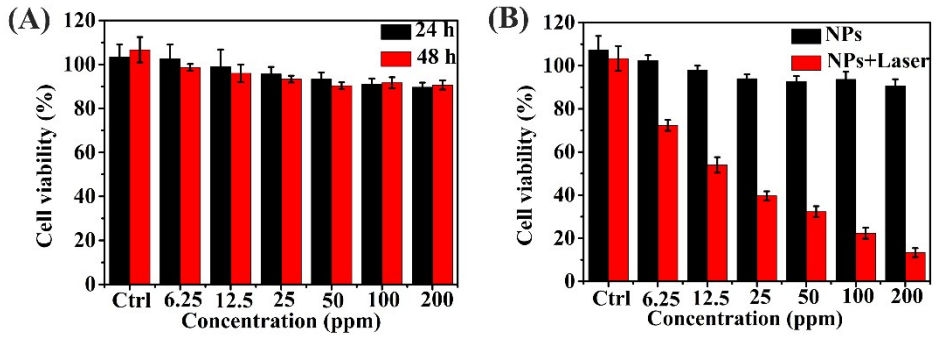

Figure S10. (A) Cytotoxicity of the HCCuS@Spiky Au NPs in HeLa cells after 24 and 48 h incubation. (B) Viability of HeLa cells incubated with HCCuS@Spiky Au NPs at varying concentration.

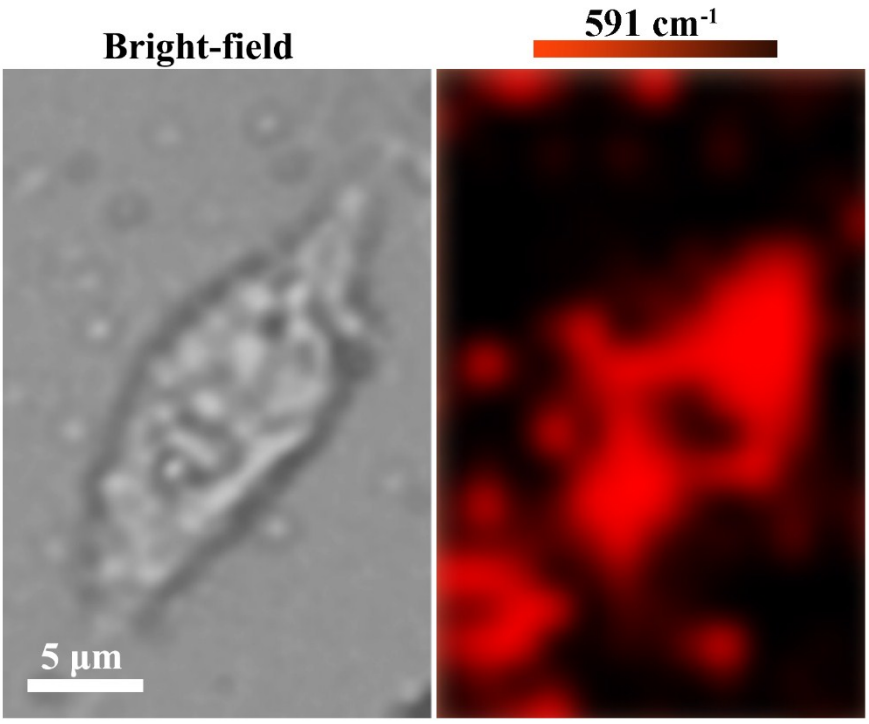

Figure S11. Bright-field and SERS mapping images of HeLa cells incubated with CVa-coated HCCuS@Spiky Au NPs for 6 h.

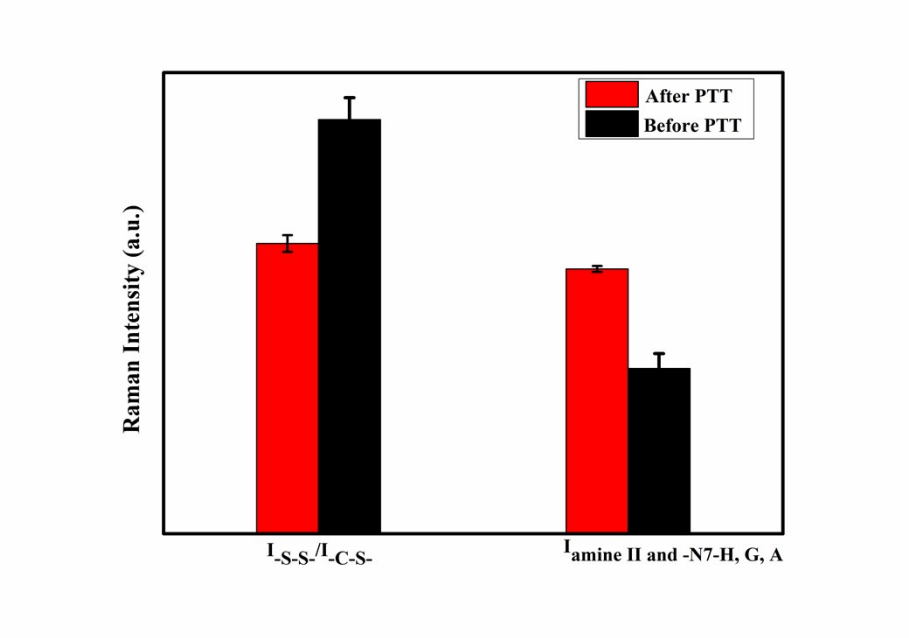

Figure S12. Plot showing changes in the SERS band intensities for the ratio of the -S-S- and -C-S- vibrations, normalized amine II, -N_7-H, G, A vibrations before and after PTT.

Table S1: Assignment of SERS spectral bands.

Shift (cm^{-1})	Component	SERS band assignment
495-510	Protein	-S-S-
640-675	Protein	-C-S-
820-850	Lipid and Proteins	Liquid symmetric –O-C-C-N-stretch and Tyr
1000-1010	Protein	Phe ring breathing
1020-1030	Protein	Phe C-H in-plane bending and Trp ring breathing
1120-1140	Liquid and Protein	C-N backbone and Liquid trans-conformations
1170-1190	Protein	C-H bend, C-C stretch, Tyr
1200-1210	Protein	C_6H_5-C stretch of Phe and Tyr
1215-1225	Protein	Amide III (β-sheet)
1265-1300	Protein	Amide III (α-helix)
1300-1325	Protein and Liquid	-CH_2 twist
1400-1460	Protein, DNA	C-H deformation, Amide II, G, and A
1584-1592	DNA	-N_7-H, G, A

References

[1] C. Noguez. J. Phys. Chem. C. 2007, 111, 3806.
[2] K. L. Kelly, E. Coronado, L. L. Zhao, G. C. Schatz, J. Phys. Chem. B., 2003, 107,668.
[3] M. W. Ji, M. Xu, W. Zhang, Z. Z. Yang, L. Huang, J. J. Liu, Y. Zhang, L. Gu, Y. X. Yu, W. C. Hao, P. F. An, L. R. Zheng, H. S. Zhu, J. T. Zhang, Adv. Mater., 2016, 28, 3094.
[4] W. Knoll, Annu. Rev. Phys. Chem., 1998, 49, 569.
[5] A. A. Lazarides, G. C. Schatz, J. Chem. Phys., 2000, 112, 2987.
[6] S. Link, M. A. EI-Sayed, J. Phys. Chem. B., 1999, 103, 4212.
[7] S. Barbosa, A. Agrawal, L. Rodríguez-Lorenzo, I. Pastoriza-Santos, R. A. Alvarez-Puebla, A. Kornowski, H. Weller, L. M. Liz-Marzán, Langmuir., 2010, 26, 14943.
[8] P. S. Kumar, I. Pastoriza-Santos, B. Rodríguez-González, F. J. García de Abajor, L. M. Liz-Marzán, Nanotechnology., 2008, 19, 1.
[9] N. E. Motl, J. F. Bondi, R. E. Shaak, Chem. Mater., 2012, 24, 1552.
[10] C. H. Kuo, T. E. Hua, M. H. Huang, J. Am. Chem. Soc., 2009,131, 17871.
[11] X. G. Ding, C. H. Liow, M. X. Zhang, R. J. Huang, C. Y. Li, H. Shen, M. Y. Liu, Y. Zou, N. Gao, Z. J. Zhang, Y. G. Li, Q. B. Wang, S. Z. Li, J. Jiang, J. Am. Chem. Soc., 2014, 136, 15684.
[12] H. Sun, J. T. He, J. Y. Wang, S. Y. Zhang, C. C. Liu, T. Sritharan, S. Mhaisalkar, M. Y. Han, D. Wang, H. Y. Chen, J. Am. Chem. Soc., 2013, 135, 9099.
[13] X. R. Deng, K. Li, X. C. Cai, B. Liu, Y. Wei, K. R. Deng, Z. X. Xie, Z. J. Wu, P. A. Ma, Z. Y. Hou, Z. Y. Cheng, J. Lin, Adv. Mater., 2017, 29, 1701266.